Elucidating synergistic dependencies in lung adenocarcinoma by proteome-wide signaling-network analysis

Mukesh Bansal[1,2,*#], Jing He[3,4,5,*], Michael Peyton[6*], Manjunath Kaustagi[3], Archana Iyer[3], Michael Comb[10], Michael White[6], John Minna[11], Andrea Califano[3,4,5,7,8,9,#]

[1] Psychogenics Inc. Tarrytown, New York, USA
[2] Department of Neuroscience, Icahn School of Medicine at Mount Sinai, New York
[3] Department of Systems Biology, Columbia University, New York, NY
[4] Center for Computational Biology and Bioinformatics (C2B2), Columbia University, New York, NY, USA
[5] Department of Biomedical Informatics (DBMI), Columbia University, New York, NY, USA
[6] Department of Cell Biology, University of Texas Southwestern Medical Center, Dallas, TX 75390, USA
[7] Department of Biochemistry and Molecular Biophysics, Columbia University, New York, NY
[8] Institute for Cancer Genetics, Columbia University, New York, NY
[9] Herbert Irving Comprehensive Cancer Center, Columbia University, New York, NY
[10] Cell Signaling Technology, 3 Trask Lane, Danvers, MA 01923, USA
[11] Hamon Center for Therapeutic Oncology Research, Simmons Comprehensive Cancer Center, Departments of Pharmacology, and Internal Medicine, University of Texas Southwestern Medical Center, Dallas, Texas

* These authors contributed equally
[#] Correspondence should be address to M.B (mukesh.bansal@psychogenics.com); A.C. (ac2248@cumc.columbia.edu)

Summary

Signaling pathway models are largely based on the compilation of literature data from heterogeneous cellular contexts. Indeed, *de novo* reconstruction of signaling interactions from large-scale molecular profiling is still lagging, compared to similar efforts in transcriptional and protein-protein interaction networks. To address this challenge, we introduce a novel algorithm for the systematic inference of protein kinase pathways, and applied it to published mass spectrometry-based phosphotyrosine profile data from 250 lung adenocarcinoma (LUAD) samples. The resulting network includes 43 TKs and 415 inferred, LUAD-specific substrates, which were validated at >60% accuracy by SILAC assays, including "novel' substrates of the EGFR and c-MET TKs, which play a critical oncogenic role in lung cancer. This systematic, data-driven model supported drug response prediction on an individual sample basis, including accurate prediction and validation of synergistic EGFR and c-MET inhibitor activity in cells lacking mutations in either gene, thus contributing to current precision oncology efforts.

Keywords: signaling network, lung cancer, tyrosine kinase, combination therapy, proteomics, EGFR, c-MET

Introduction

Lung adenocarcinoma (LUAD) is a leading cause of cancer related deaths in United States, representing 40% of 225,500 new lung cancer cases every year, and has a 5-year survival rate of only 16 % (1). Excluding immunotherapeutic agents, which have recently shown significant success in a relatively small subset of patients (2), the most effective targeted therapies for this diseases were designed to inhibit tyrosine kinase proteins harboring genetic alterations that induce aberrant activation of downstream pathways (3-7). These the most frequent such actionable alterations include EGFR mutations and ALK-EML4 fusion events, in ~15% and ~3-7% of LUAD patients, respectively (8, 9). Yet, while targeted therapy is initially effective in a significant fraction of tumors harboring these genetic alterations, the vast majority of treated patients will either fail to respond or will develop resistance to mono-therapy (10, 11). In addition, most patient lack actionable alterations altogether. This suggests that novel approaches are critically needed.

A possible alternative to minimize emergence of resistance is combination therapy, a strategy that has been shown to be effective in many metastatic tumors, such as breast cancer and acute myeloid leukemia (12-14). However, systematic identification of effective drug combinations on a genetic alteration basis is difficult, because the number of patients presenting multiple actionable events is extremely low. As a result, combination therapy is generally hypothesized and tested on an empirical basis or based on elucidation of complex mechanisms of tumor cell adaptation. In addition, accurate prediction of response to available mono-therapy – including to EGFR inhibitors – in patients lacking any genetic alteration represents an equally relevant challenge, especially since a small fraction of $EGFR^{WT}$ patients have been shown to respond to Afatinib, even though a predictive biomarker is not available. To address these limitations, we and other have proposed that rational design of combination therapy and the identification of critical targetable

63 dependencies may require a more mechanistic and tumor-context-specific understanding of the
64 molecular interactions that underlie their potential synergistic activity, starting with tyrosine
65 kinases, which represent a critical class of pharmacological targets in cancer (15). Such an
66 approach requires methodologies for the accurate and systematic elucidation of tumor-specific
67 signaling transduction pathways.

68 Dissection of signal transduction networks represents a complex endeavor, requiring elucidation
69 of hundreds of thousands of tissue-specific molecular interactions that mediate the post-
70 translational modification of protein substrates. *In vitro* approaches generally fail to capture the
71 tissue-specific nature of these interactions, thus providing "average" signal transduction pathways
72 that are both incomplete and inaccurate. In addition, experimental approaches that have been
73 successful in accelerating the analysis of molecular interactions in transcriptional regulation and
74 protein-protein interaction in stable-complexes, such as those based on co-expression or yeast-
75 2-hybrid assays, do not easily translate to elucidating signaling interactions. Similarly, approaches
76 based on the use of phospho-specific antibodies, while elegant and effective, are limited to only
77 a handful of proteins. Computationally, compared to the many algorithms that have been
78 developed for the reverse engineering of transcriptional and protein-complex interactions (16, 17),
79 only a handful of experimentally validated algorithms are available for the dissection of signaling
80 networks, none of which works at the proteome-wide level or is tumor-context specific (16, 18,
81 19).

82 Recent availability of proteome-wide molecular profile data, characterizing the abundance of
83 phospho-tyrosine-enriched peptides by liquid chromatography coupled to tandem mass
84 spectrometry (LC-MS/MS), suggests that additional methodologies may be developed to extend
85 approaches that have been successfully applied to the dissection of transcriptional networks from
86 gene expression profiling. In this manuscript, we propose extending the Algorithm for the
87 Reconstruction of Accurate Cellular Networks (ARACNe) (20) for the reverse engineering of

88 signal transduction networks from large-scale phosphoproteomic profiles. The new method,
89 *pARACNe*, addresses critical issues that prevented the direct application of the original ARACNe
90 algorithm on phosphoproteomic profile data. Briefly, the new algorithm addresses critical
91 computational challenges presented by LC-MS/MS and spectral counting data, while
92 incorporating enzymatic signaling characteristics into the algorithm design. In particular,
93 pARACNE is designed to handle three critical issues resulting from the use of LC-MS/MS assays,
94 including the highly sparse nature of phosphopeptide abundance data, the large amount of noise
95 and missing data, and the degenerate peptides-to-protein mapping.

96 We applied pARACNE to the analysis of previously published, genome-wide phosphoproteomic
97 data from 245 lung adenocarcinoma (LUAD) samples, including 151 fresh-frozen biopsies, 46 cell
98 lines, as well as 48 normal lung tissues. The resulting network comprised 46 tyrosine kinases
99 (TK) densely connected with 415 candidate substrates (including 377 proteins lacking any TK
100 activity), representing the first genome-wide, tumor-context-specific model for a TK signal
101 transduction network, capturing both protein-specific and phospho-site specific events. We
102 validated substrate predictions for two "hubs," whose activity may play a key role in determining
103 sensitivity to Erlotinib and Crizotinib, two FDA-approved drugs for LUAD, including the EGFR and
104 c-MET tyrosine kinases by independent SILAC assays and database analysis, with >60%
105 accuracy. Of particular note, the inferred TK-substrate network provided unique information about
106 tyrosine kinase auto-phosphorylation events, either direct (cis) or via a second kinase (trans).

107 Analysis of the resulting TK-network – by extending the VIPER (Virtual Proteomics by Enriched
108 Regulon analysis) algorithm (21), an established method for the inference of Master Regulator
109 proteins – recapitulated established genetic determinants of LUAD and was effective in predicting
110 sensitivity to Erlotinib and Crizotinib combination therapy. Predicted sensitivities were validated
111 in an independent set of LUAD cell lines, the majority of which harbored no genetic alterations in
112 the corresponding genes. Furthermore, predictions based on the analysis of the corresponding

113 patient cohort were strongly supported by genomic information, suggesting potential value in
114 using these analyses for the identification of effective combination therapies in precision oncology.

115

116 Results

117 *Overview of the pARACNe Algorithm*

118 Enzymatic activity of tyrosine kinase (TK) proteins – as assessed by the ability to phosphorylate
119 their downstream substrates – is effectively determined by their phosphorylated isoform
120 abundance (**Fig. 1A, B**). Therefore, we reasoned that computational inference of TK-substrate
121 interactions (**TK→S**) could be effectively performed by measuring dependencies between their
122 respective phospho-states by mutual information analysis (22) over a large sample compendium
123 **(Fig. 1C)**. Unfortunately, due to signal transduction cascade complexity and pathway cross-talk,
124 such dependencies can manifest between protein pairs that are not involved in direct **TK→S**
125 interactions. The ARACNe algorithm – previously designed for the reverse engineering of
126 transcriptional networks – effectively addresses this problem by leveraging the Data Processing
127 Inequality (23). This is a critical property of the mutual information that effectively allows
128 disambiguating between direct and indirect interactions by assessing whether information transfer
129 on any candidate direct interaction (e.g., $\mathbf{TK_1 \rightarrow S}$) is greater than transfer on every other indirect
130 path (e.g., $\mathbf{TK_1 \rightarrow TK_2 \rightarrow S}$). ARACNe has been highly successful in the experimentally validated
131 dissection of transcriptional networks via analysis of large gene expression profile compendia.
132 ARACNe-inferred targets of transcription factors were validated in multiple cellular contexts, with
133 an accuracy of 70% to 80% (20, 24-27).

134 However, ARACNe relies on molecular profile data that is both continuous and non-sparse,
135 properties that are not always provided by quantitative proteomic data sets, which can be

136 generated by a variety of methods. Those based on LC-MS/MS represent the most popular
137 approaches (28), but different implementations have specific performance profiles in terms of
138 analyte throughput, consistency of measurement of peptides across samples and linear dynamic
139 range (29). Depending on the data acquisition method, one or both of these assumptions of
140 ARACNe are violated in proteome-wide datasets generated by the most popular methods based
141 on data-dependent acquisition. Particularly when employing quantification by spectral counting,
142 as is typically conducted for global protein-protein interaction studies (30, 31), phosphoproteomic
143 data is both discrete (i.e., generally represented by spectral counts) and very sparse, with a
144 majority of peptides having zero spectral counts and presenting a significantly skewed distribution
145 for low-abundance peptides.

146

147 To address these limitations, we developed a phospho-proteomic specific algorithm, pARACNe
148 (phospho-ARACNe) (**Fig. 1C**), specifically designed to measure phospho-state dependencies
149 between TKs and their candidate substrates from large-scale LC-MS/MS phosphoproteomic
150 profiles. pARACNe thus extends the original ARACNe framework to allow systematic inference
151 of **TK→S** interactions. Specifically, to handle the highly discrete nature of the data, we replaced
152 the kernel-density and adaptive partitioning based mutual information estimators in the original
153 algorithm with a bin-count based method (**Fig. 1C4**), using gold standard data to select the most
154 effective number of bins [12] (see Methods). Furthermore, to deal with the skewed spectral count
155 distribution, we introduce an iterative quantile discretization method, where samples are binned
156 together, based on their spectral counts, to produce a distribution as close to uniform as possible
157 (**Fig. 1C3,** Methods).

158

159 ***pARACNe-inferred LUAD-specific TK-phosphorylation Network***

160 We used pARACNe to reconstruct a LUAD-specific TK-signaling network, by analyzing
161 phosphopeptide profiles obtained from 245 LUAD samples from Guo et al. (32). These data
162 represent the abundance of peptides containing at least one phospho-tyrosine, as obtained by
163 phosphoproteomic analysis of 46 LUAD cell lines, 151 LUAD tumors, and 48 adjacent normal
164 samples. LC-MS/MS profiling produced spectral counts for 3,920 phospho-tyrosine containing
165 peptides mapping to ~2,600 different proteins. Based on these data, pARACNE identified 2,611
166 candidate phospho-peptide/phospho-peptide dependencies, which could be further mapped to
167 2,064 unique **TK→S** interactions (**Table S1, S2)**. These represent interactions between 46 unique
168 TKs and their candidate substrates. These include 174 $\mathbf{TK_1 \rightarrow TK_2}$ interactions between two TKs
169 (**Fig. 2A**), representing a statistically significant bias toward TK-TK interactions in the network
170 ($p = 10^{-62}$). This suggests that, within the complete TK signaling network, TKs themselves may
171 form a more densely inter-connected subnetwork than previously assessed, providing potentially
172 valuable novel information about adaptive response, pathway cross-talk, and auto-regulatory
173 loops.

174 Such highly interconnected structure provides potential functional advantage compared to less
175 interconnected (i.e., "flat") architectures, including the ability to provide more fine-grain response
176 to a highly heterogeneous variety of exogenous signals and conditions, the ability to provide rapid
177 adaptive response to changing stimuli, and the ability to preserve cell state via autoregulatory
178 feedback. Consistent with the underlying biology, and in contrast to transcriptional networks, the
179 vast majority of pARACNe-inferred interactions have a positive Spearman correlation, with higher
180 counts of TK-mapped phosphopeptides corresponding to higher counts of candidate substrate-
181 mapped ones. This is consistent with the fact that TKs only phosphorylate their substrates, thus
182 inducing positive phospho-state correlation. Only a negligible number of inferred interactions
183 (0.5%) were associated with a negative Spearman correlation ($N = 11$, $p \leqslant 0.05$). These may

184 represent either indirect interactions where the TK activates a substrate-specific phosphatase or
185 direct interactions where phosphorylation of one phosphosite may prevent phosphorylation of
186 another site on the same protein.

187

188 ***LUAD Network Accuracy and Sensitivity Analysis***

189 To estimate the accuracy of the inferred TK-signaling network, we investigated the substrates of
190 two TK-proteins, EGFR and c-MET, representing high-affinity binding targets of existing FDA-
191 approved TK inhibitors for LUAD. Specifically, we compared their pARACNe-inferred substrates
192 to those reported in the phosphoDB database (33) and those supported by experimental
193 evidence, based on previously published SILAC assays, following cell line treatment with
194 associated, selective TK inhibitors. pARACNe inferred 123 EGFR substrates (**Fig. 2B**). Of these,
195 5 (blue and cyan) were included as high-confidence EGFR substrates in phosphoDB, out of 13 in
196 total (38%), including the established EGFR auto-phosphorylation site. Moreover, 50 additional
197 proteins (45%, green) showed significant decrease (at least 2 fold) in the abundance of their
198 phosphorylated isoforms in SILAC assays (32), following treatment of H3255 cells with the EGFR
199 inhibitor Gefitinib. Similarly, pARACNe predicted 179 c-MET substrates (**Fig. 2C)**. Notably, both
200 of the established substrates reported in PhosphoDB were identified by pARACNE (100%, blue).
201 Moreover, 126 additional proteins (71.5%, blue) showed significant decrease in the abundance
202 of their phosphorylated isoforms in SILAC assays(32), following treatment of MKN45 cells with
203 the first-generation c-MET-specific inhibitor Su11274.

204 We used MKN45 to assess overall prediction accuracy, even though it represents a gastric cancer
205 cell line, because signaling networks should are much more conserved across tissue contexts
206 than transcriptional ones. Indeed, while lineage-specific chromatin state represents a major
207 determinant of transcriptional regulation, it only affects signal transduction in terms of overall

208 protein availability. As a result, it is reasonable to expect that an even greater overlap of inferred
209 vs. SILAC positive substrates may be achieved in native LUAD cells.

210

211 Taken together, these data suggest that pARACNe can identify a much larger subset of candidate
212 substrates, while both identifying a significant proportion of established substrates (46% on
213 average, based on phosphoDB) and maintaining high accuracy (~60% on average, by SILAC
214 assays). This also suggest that, similar to transcription factor targets reported in the literature, TK
215 substrates are still poorly characterized in existing repositories, even for highly relevant and
216 exceedingly well-studied kinases such as EGFR and c-MET. As a result, pARACNe could provide
217 significant novel hypotheses for TK→S interactions that can be validated as required. We should
218 also note that the reported accuracy for pARACNe is estimated using SILAC data on a single cell
219 line. SILAC assays have significant false negatives and it would be reasonable to expect that,
220 once tested in additional cell lines, the accuracy of pARACNe could further increase. As a further
221 performance benchmark, we used the same SILAC benchmark to test predictions by NetworkIN,
222 a reverse engineering method based on protein sequence motif analysis and protein association
223 networks (16). The analysis found almost no consensus with SILAC assays, with only one out of
224 33 NetworkIN-predicted EGFR substrate identified as significantly dephosphorylated following
225 treatment with TK-specific inhibitors.

226

227 ***Systematic, Network-based Inference of Pharmacological Dependencies***

228 Once an accurate model of signal transduction in LUAD cells was established by pARACNe
229 analysis, we interrogated the corresponding TK→S network using phosphoproteomic signatures
230 from 46 LUAD cell lines to identify key dependencies for experimental validation. For this purpose,
231 we extended the VIPER algorithm (Virtual Proteomics by Enriched Regulon analysis)(21), which

232 was originally developed to identify the MR proteins that mechanistically regulate the
233 transcriptional state of a tumor by assessing the enrichment of their transcriptional targets in
234 differentially expressed genes in the tumor signature. VIPER and its predecessor MARINa
235 (Master Regulator Inference algorithm) (34) have been instrumental in inferring MR proteins
236 representing key functional determinants of tumor-related phenotypes in many cancer types, from
237 glioblastoma (26, 27, 35), neuroblastoma (34), lymphoma (36, 37), and leukemia (38) to prostate
238 (39-41) and breast adenocarcinoma(42-44), among others. We thus reasoned that VIPER could
239 be modified to identify master regulator TKs, most likely to mechanistically regulate the differential
240 phosphorylation pattern observed in a specific tumor sample (**Fig. 3A**). A specific additional value
241 of the algorithm is that, as previously shown {Lefebvre, 2010 #1763}{Aytes, 2014 #2520}{Carro,
242 2010 #4021}, it could not only identify MR TK proteins, representing individual, pharmacologically
243 accessible dependencies of the tumor, but also TKs representing potential synergistic MR-pair as
244 candidate dependencies for combination therapy.

245 VIPER can be easily modified to analyze phosphoproteomic signatures (pVIPER). Specifically,
246 rather than assessing the enrichment of a protein's transcriptional targets (regulon) in differentially
247 expressed genes, pVIPER is designed to measure the enrichment of a TK's substrates (signalon)
248 in differentially phosphorylated proteins. Since inferred TK-substrate interactions are virtually all
249 positive, this further increases the accuracy of the algorithm by supporting use of a single-tail
250 enrichment analysis as opposed to the three-tail analysis of the original implementation. We first
251 performed pVIPER analysis at the individual phosphopeptide level, rather than by averaging
252 phosphopeptide state on a whole protein level. We then combined the result of the analysis across
253 all phosphopeptides mapping to the same protein. Consistent with VIPER's experimentally
254 validated ability to identify synergistic master regulators proteins by transcriptional network
255 analysis, pVIPER inferred several candidate synergistic TK interactions based on the statistical
256 significance of the signature-enrichment of substrates shared by both TKs compared to that of

257 substrates uniquely mapped to either one or the other TK (see Method section). Systematic
258 VIPER analysis of phosphoproteomic profiles from 46 LUAD cell lines generated between 2 and
259 13 master regulator TKs or synergistic TK-pairs, as candidate pharmacologically actionable
260 dependencies, for each cell line, thus generating a plausible number of hypothesis for each cell
261 line (**Fig. 3B** and **Fig. 3C**).

262

263 **pVIPER Identifies LUAD-specific Dependencies**

264 pVIPER analysis inferred several TK proteins as highly conserved individual dependencies across
265 multiple cell lines, including the Ephrin type-A receptor 2 (*EPHA2*), epidermal growth factor
266 receptor (*EGFR*), c-Met proto-oncogene (*MET*), and HER2 receptor tyrosine kinase 2 (*ERBB2*),
267 suggesting a critical role of these proteins in the maintenance of LUAD cell line state. This is also
268 in agreement with the functional role of these genes and the use of inhibitors of these kinases
269 across a large panel of patients in multiple cancer types (45-49).

270 In contrast to these established LUAD cell line dependencies, we also identified several TKs as
271 dependencies of specific cell lines. This can either be the result of associated genetic or
272 epigenetic alterations in these cell lines or the result of field effects, where multiple genetic
273 alterations or alterations in upstream pathway contribute to the cell line dependency on a specific
274 TK activity. For instance, we identified ALK (Anaplastic Lymphoma Receptor Tyrosine Kinase) to
275 be addiction point only in H2228 cell line. ALK is a conserved trans-membrane receptor tyrosine
276 kinase (RTK) protein in the insulin-receptor super family. Chromosomal alterations involving *ALK*
277 translocations and fusion events have been identified in several cancer types including LUAD (50,
278 51), diffuse large B-cell lymphomas (52), neuroblastoma (53), and inflammatory myofibroblastic
279 tumors (54), among others. Additionally, ALK fusion events with other genes, including EML4
280 (Echinoderm Microtubule-associated protein Like 4) in LUAD lead to aberrant protein activity

281 eliciting “oncogene addiction” (51). Presence of ALK-EML4 fusion transcripts, in ~3–7% of LUAD
282 patients (55-57), is a strong predictor of response to ALK inhibitors, such as Crizotinib, among
283 others (58, 59). Interestingly, among all available LUAD cell lines for which a phosphoproteomic
284 profile was available, H2228 was the only one with an established ALK-EML4 fusion event and
285 with established sensitivity to ALK inhibitor (60, 61). This further reflects the specificity of our
286 analysis as this was the only cell line predicted to depend on ALK activity. Interestingly, we
287 identified 4 additional H2228 dependencies, namely EGFR, Epha2, c-MET, and PTK2. H2228
288 sensitivity to EGFR inhibitors, in combination with ALK inhibitors, was already established (61).
289

290 ***EGFR and c-MET are Predicted Dependencies in Multiple LUAD Cell Lines***

291 As discussed, pVIPER analysis revealed several TK-pairs as candidate synergistic dependencies
292 across several cell lines, such as Epha2/c-MET, EGFR/PTK2, EGFR/Epha2, Epha2/c-MET, and
293 EGFR/c-MET. Among these the EGFR/c-MET pair emerged as the most conserved synergistic
294 TK-pair across the available cell lines. In addition, EGFR and c-MET were also identified as
295 candidate TK MRs in several of these cell lines, suggesting either a complementary or synergistic
296 role for these proteins and a potential therapeutic opportunity for combination therapy in LUAD
297 (62, 63).
298

299 To validate pVIPER-predicted, cell line specific EGFR/c-MET synthetic lethality, we selected a
300 panel of 14 cell lines, 11 of which were predicted to be synergistically dependent on EGFR/c-MET
301 (H226, H2122, H1666, H2172, Cal-12T, H2023, H1568, Calu-3, H1650, HCC78, and A549), as
302 well as 3 negative controls with no predicted synergistic or individual dependencies on the two
303 TKs (H2170, H460, and H520). To measure sensitivity to these agents, we used two different and
304 complementary assays, including: (a) colony formation assay to assess long term sensitivity (**Fig.
305 4A and Methods**) and (b) 3-[4,5-dimethylthiazol-2-yl]-2,5 diphenyl tetrazolium bromide (MTS)
306 assay for short term sensitivity analysis (**Fig. 5A, Table S3 and Methods**). For colony formation

307 assays, cells were treated with either an EGFR inhibitor (Erlotinib, 1uM) or a c-MET/ALK inhibitor
308 (Crizotinib, 0.1uM), either individually or in combination (see Methods). To evaluate synergistic
309 dependency on EGFR/c-MET we used Excess Over Bliss (64), which measures the difference
310 between the observed effect on colony formation and the effect expected from a purely additive
311 model. For MTT assay, first, cells were treated with EGFR inhibitor (Erlotinib) or MET inhibitor
312 (Crizotinib) individually at various concentrations to identify IC50 (concentration resulting in 50%
313 cell death). Next, cells were treated with 1 uM of Erlotinib and varying concentrations of Crizotinib
314 to identify combinations resulting in IC50 and used the combination index (CI) statistic (65) to
315 measure interaction between the two drugs.
316
317 Across all 11 cell lines tested in colony formation assay, 8 showed significant sensitivity to either
318 individual inhibitors ($H226_{E,C}$, $H2122_{E}$, $H1666_{E,C}$, $Cal\text{-}12T_{E}$, $Calu\text{-}3_{E,C}$, $H1650_{E}$) or synergistic
319 sensitivity to the combination ($HCC78_{E+C}$ and $H2023_{E+C}$) (**Fig. 4B-C)**. Surprisingly, all of these cell
320 lines were $EGFR^{WT}$, ALK^{WT}, and $c\text{-}MET^{WT}$, except for H1650, which was $EGFR^{Mut}$. Thus, based
321 on standard of care criteria, 7 out of 8 cell lines would not have been considered as sensitive to
322 either EGFR or ALK/c-MET inhibitors. Several cell lines presented striking sensitivity to either one
323 ($H2122_{E}$, $Cal\text{-}12T_{E}$, $H1650_{E}$) or both inhibitors ($H226_{E,C}$, $H1666_{E,C}$, $Calu\text{-}3_{E,C}$) in isolation, thus
324 making the assessment of synergistic drug sensitivity difficult. In addition, three $EGFR^{WT}$ cell lines
325 harboring BRAF (Cal-12T and H1666) or KRAS (H2122) mutations were also highly sensitive to
326 Erlotinib as a single agent, as predicted by pVIPER, despite the fact that KRAS pathway mutations
327 are mutually exclusive with EGFR mutations and predictive of Erlotinib resistance (**Fig. 4C**).
328 Finally, none of these cell lines was predicted to be sensitive to ALK inhibitors, suggesting that
329 Crizotinib sensitivity is mediated by c-MET specific dependencies. Of the negative controls, only
330 one (H2170) showed high sensitivity to Erlotinib. Taken together, 8/11 cell lines (73%) predicted
331 as sensitive to the inhibitors were validated long term colony formation assays, while only 1/3
332 negative controls showed sensitivity to these agents (33%).

333

334 To evaluate the short-term interaction between EGFR and c-MET, we performed MTT assay
335 across 11 cell lines (HCC78, H2023, H1650, Calu-3, H2172, H2122, H1568, A549, H1666, H520
336 and H2170) including 2 negative control cell lines (H520 and H2170). Similar to colony formation
337 assay, we found synergistic sensitivity to EGFR and c-MET inhibitors in 6/9 cell lines (67%), with
338 5 cell lines showing strong synergy (CI ≤ 0.8) (**Fig. 5B-C**) and 1 borderline synergy (CI = 0.82),
339 showing the consistency between two assays. However, for two cell lines, H1666 and H2170 (a
340 negative control), results were inconsistent between long term colony formation and MTT assays.
341 For both H1666 and H2170 cell lines, colony formation and MTT assay to showed sensitivity to
342 Erlotinib alone, where colony formation assay has complete abrogation of colonies at 1 μM of
343 Erlotinib, and later had IC_{50} =1.25 μM and 3.7 μM for H1666 and H2170 respectively. However,
344 in combination therapy, MTT assay showed antagonism (CI >1), despite the fact that colony
345 formation assay still showed complete abrogation which could be associated to the accumulation
346 of new mutations in these cell lines. However, this is just hypotheses and needs to be verified by
347 further experiments such as sequencing of these cell lines pre-and post-treatment.

348

349 ***Phosphosite-specific Phosphorylation Predicts EGFR/c-MET Inhibitor Synergy.***

350 In previous section, we assessed the pVIPER predictions after consolidating the result at protein
351 level. Following the results from MTT and colony formation assays, we reanalyzed the pVIPER
352 predictions at the phosphopeptide level. Interestingly, this revealed that whenever synergistic
353 EGFR/c-MET dependencies were predicted from phosphosite $EGFR_{1197}$ and phosphosites other
354 than $c\text{-}MET_{1003}$ (H1666, Cal-12T, H1650), cell lines responded to Erlotinib in isolation, while when
355 predictions were based on phosphosites $EGFR_{1197}$ and $c\text{-}MET_{1003}$ (HCC78, H2023, and Calu-3),
356 cells exhibited bona fide synergistic sensitivity to the two inhibitors, with the only possible
357 exception of Calu-3, which showed synergistic sensitivity in MTT assays and additive sensitivity
358 to both inhibitors in colony formation assays. Conversely, when predictions were not based on

359 either phosphotyrosine, cells exhibited no sensitivity to the individual inhibitors or the combination
360 (H2172, H226, A549, H460, H520, H1568). Thus, predictions based on these two phosphosites
361 produced no false positives (6 out of 6 predicted and validated as non-sensitive) and only 2 false
362 negatives (H2170 and H2122), resulting in an error rate of only 2 out of 14 cell lines (14%, $p =$
363 0.0093 using fisher exact test).
364
365 This finding is in agreement with the established role of $EGFR_{1197}$ as a predictor of EGFR inhibitor
366 sensitivity (66). Intriguingly, when sensitivity was predicted using phosphosites other than
367 $EGFR_{1197}$ and $c\text{-}MET_{1003}$, cell lines did not respond to the inhibitors, either individually or in
368 combination. For these two peptides, we found their common substrates to be hyper
369 phosphorylated in the sensitive cell lines **(Fig. 6A**) compared to the specific substrates of each of
370 them, whereas cell line responding only to EGFR inhibitors showed more hyper phosphorylation
371 of EGFR only substrates (**Fig. 6B**). Cell lines resistant to both EGFR and c-MET inhibitors either
372 showed no change in the phosphorylation status or hypo-phosphorylation compared to the normal
373 samples (**Fig. 6C**). Hence, either the common substrates of EGFR and c-MET, or the
374 phosphorylation status of $EGFR_{1197}$ and $c\text{-}MET_{1003}$ could potentially be used as biomarkers for
375 predicting therapy with the dual inhibitors. However, this conclusion is based on a very limited
376 number of observations and lacks the statistical power. This finding needs a re-
377 evaluation/validation using larger cohort of samples to establish an appropriate biomarker for
378 combination therapy.
379
380 ***Systematic Inference of Patient-specific Dependencies***
381 Similar to cell lines, when applied on patient data (32), pVIPER identified EGFR as one of the
382 most common addiction points (**Fig. 6**). We inferred EGFR dependency in 12 patients. Of these,
383 5 harbored EGFR mutations, while the remaining 7 patients had not been tested for this mutation,
384 showing a high consistency between our predictions and the genetic predisposition for sensitivity

385 to EGFR inhibitors. In the entire cohort, there were only 3 patients with EGFR mutations that were
386 not identified as EGFR dependent by pVIPER, resulting in an overall sensitivity of 62.5% (5/8).
387 However, it is well known that >50% of patients harboring EGFR mutations do not respond to
388 Erlotinib, suggesting that these may not be false negatives but rather patients with low activation
389 of downstream EGFR pathways, despite their $EGFR^{Mut}$ state. Similarly, our analysis identified
390 candidate ALK dependencies in 4 patients. Of these one had an established TFG-ALK fusion,
391 whereas the others had not been tested for ALK fusion events.

392 Across all patient samples, we observed Discoidin Domain Receptor-1 (DDR1) to be the most
393 frequent addiction point, which was not predicted for any of the 46 cell lines. One reason for the
394 difference is that DDR1 is collagen dependent and there may be differences in the 3D structure
395 of the tumor and the cell lines growing on the plate. An independent study (67) in a cohort of 83
396 lung cancer specimens found that silencing of DDR1 in these samples leads to the hampering of
397 cell survival, reduced invasiveness in collagen matrices, increased apoptosis in basal condition
398 and decreased metastatic activity in model of tumor metastasis to bone, signifying it as a potential
399 novel therapeutic target.

400 Discussion

401 In this paper, we developed pARACNe to infer Tyrosine Kinase (TK) signaling network using
402 published genome-wide phosphoproteomic data from lung cancer. The network prediction was
403 validated using SILAC experiments, with high accuracy. Interrogation of the predicted TK-
404 substrate network generated biologically meaningful hypotheses, followed by experimental
405 validations illustrating the effectiveness of predicted kinase inhibitor combination, EGFR and c-
406 MET combination inhibitors, in treating lung cancer cell lines. Furthermore, Master Regulator
407 Analysis using patient proteomics data provides implications for using targeted agent
408 combinations to treat patients based on their proteomic profile data.

409

410 Notably, pARACNe is significant and powerful as of its genome-wide scale and context-specificity
411 in discovering global signaling cascading relationships, which were missing by previous methods.
412 For example, methods proposed by Linding et al. (16) combine motif-based phospho-site
413 predictions with information of physical association, co-occurrence, and co-expression to identify
414 substrates with high specificity and accuracy, but with low coverage and lack of contextual
415 specificity. Bender et al (17) used reverse phase protein assay data after various stimulations to
416 cells and inferred signaling network using hidden Markov models and genetic algorithms. Even
417 though the resulting networks are context specific, they lack genomic-scale coverage. There have
418 been methods which used existing large-scale protein networks and prune them using
419 transcriptomic information to identify signaling pathways (68-70). In addition, attempts have been
420 made to reconstruct signaling network using gene expression data (71, 72). However, as signaling
421 complexity lies mostly in upper level of cellular processes, inferring the cascades from
422 downstream gene expression fails to capture all the dynamics. Also, PrePPI proposed by Zhang
423 et al. (73) used protein structure-based methods to infer global protein-protein interaction, but this
424 approach fails to address phosphorylation context specificity. Innovative uses of multiplex and
425 microarray-based approaches, where multiple antibodies can be used to probe an ensemble of
426 phosphoproteins, are finally becoming sufficiently mature to allow characterization of small
427 pathways. Yet, these methods are still far from providing an unbiased, genome-wide view of
428 signal-transduction processes and continue to be completely dependent on antibody specificity
429 and availability. Similarly, assays developed specifically to monitor phosphorylation pathways,
430 such as Stable Isotope Labeling with Amino acids in Cell culture (SILAC), provides a simple and
431 straightforward approach to detect differential protein abundance. Coupled with phosphorylation
432 enriched assays, it can provide high quality quantification for post-translation phosphorylation
433 changes in cell lines. However, these methods are 1) laborious and costly; 2) can only be

434 performed to dissect the substrates of a single enzyme at a time and 3) do not differentiate
435 between direct and indirect targets.
436
437 To be noted, as the LC-MS/MS experiments used here was generated based on Tyrosine-kinase
438 enrichment, which is only about ~2% of whole phosphoproteome. pARACNe is shown only on
439 TK-substrates network. The current methodology could be extended to whole phosphoproteomic
440 data based signaling network reconstruction where the data is available. In addition to label free
441 based LC-MS/MS proteomics data used in this work, label based approaches, such as ITRAQ or
442 TMT, could generate higher throughput whole proteomic profiles which might require future
443 redesign of ARACNe to incorporate both kinases and phosphatases in regulating their
444 downstream substrates. It is reasonable to expect that a version of ARACNe developed
445 specifically to dissect signaling networks should work at least as well as its transcriptional
446 counterpart. Since the relationship between the mRNA abundance of a gene encoding a
447 transcription factor (TF) and the activity of the corresponding protein is much looser than that
448 between the abundance of a phospho-isoform of a kinase and its enzymatic activity.
449
450
451 Even though research has attempted to identify addiction points based on gene expression data
452 (74), predictions based on phosphoproteomic data appear superior in a way that they can directly
453 reflect contextual specific signaling activity and are able to be directly targeted by kinase
454 inhibitors. It is important to note that clinically, only patients with base-pair deletion at exon 19
455 (del746_A750) or a point mutation at exon 21 mutation (L858R) in EGFR shows sensitivity to
456 EGFR inhibitor such as Cedirinib or Erlotinib (75).
457

Acknowledgments

We thank George Rosenberger for manuscript advice. This work was supported by the National Cancer Institute (NCI) Cancer Target Discovery and Development program (1U01CA168426 to A.C., and 1U01CA176284 to JDM), NCI Research Centers for Cancer Systems Biology Consortium (1U54CA209997 to A.C.), NCI Outstanding Investigator Award (R35CA197745-02 to A.C.), NCI SPORE in Lung Cancer (P50CA70907 to JDM), and CPRIT (Award RP110708 to JDM).

Author Contributions

M.B. and M.K. developed the algorithm. M.B. and J.H. performed the analysis. M.P. performed the experimental validation. A.I., M.B., M. W., J.M and A.C. guided the experiments. M.B. J.H., A.I. and A.C wrote the manuscript. M.B. and A.C. provided supervision and guidance. A.C. conceived, funded and administrated the project.

Declaration of Interests

A.C.is a founder and shareholder of DarwinHealth Inc. and a member of the Tempus Inc. SAB and shareholder. Columbia University is a shareholder of DarwinHealth Inc.

473 # References

474 1. Ettinger DS, Akerley W, Borghaei H, Chang AC, Cheney RT, Chirieac LR, et al. Non-small cell lung
475 cancer. Journal of the National Comprehensive Cancer Network : JNCCN. 2012;10(10):1236-71.
476 2. Karasaki T, Nagayama K, Kawashima M, Hiyama N, Murayama T, Kuwano H, et al. Identification of
477 Individual Cancer-Specific Somatic Mutations for Neoantigen-Based Immunotherapy of Lung Cancer. J
478 Thorac Oncol. 2016;11(3):324-33.
479 3. Pasqualucci L, Kitaura Y, Gu H, Dalla-Favera R. PKA-mediated phosphorylation regulates the
480 function of activation-induced deaminase (AID) in B cells. Proc Natl Acad Sci U S A. 2006;103(2):395-400.
481 4. Fiedler D, Braberg H, Mehta M, Chechik G, Cagney G, Mukherjee P, et al. Functional organization
482 of the S. cerevisiae phosphorylation network. Cell. 2009;136(5):952-63.
483 5. Gainor JF, Varghese AM, Ou SH, Kabraji S, Awad MM, Katayama R, et al. ALK rearrangements are
484 mutually exclusive with mutations in EGFR or KRAS: an analysis of 1,683 patients with non-small cell lung
485 cancer. Clin Cancer Res. 2013;19(15):4273-81.
486 6. Janne PA, Shaw AT, Pereira JR, Jeannin G, Vansteenkiste J, Barrios C, et al. Selumetinib plus
487 docetaxel for KRAS-mutant advanced non-small-cell lung cancer: a randomised, multicentre, placebo-
488 controlled, phase 2 study. Lancet Oncol. 2013;14(1):38-47.
489 7. Mak KS, Gainor JF, Niemierko A, Oh KS, Willers H, Choi NC, et al. Significance of targeted therapy
490 and genetic alterations in EGFR, ALK, or KRAS on survival in patients with non-small cell lung cancer treated
491 with radiotherapy for brain metastases. Neuro Oncol. 2014.
492 8. Vendrell JA, Taviaux S, Beganton B, Godreuil S, Audran P, Grand D, et al. Detection of known and
493 novel ALK fusion transcripts in lung cancer patients using next-generation sequencing approaches. Sci Rep.
494 2017;7(1):12510.
495 9. Peters S, Camidge DR, Shaw AT, Gadgeel S, Ahn JS, Kim DW, et al. Alectinib versus Crizotinib in
496 Untreated ALK-Positive Non-Small-Cell Lung Cancer. N Engl J Med. 2017;377(9):829-38.
497 10. Tsvetkova E, Goss GD. Drug resistance and its significance for treatment decisions in non-small-
498 cell lung cancer. Curr Oncol. 2012;19(Suppl 1):S45-51.
499 11. Wilson FH, Johannessen CM, Piccioni F, Tamayo P, Kim JW, Van Allen EM, et al. A functional
500 landscape of resistance to ALK inhibition in lung cancer. Cancer Cell. 2015;27(3):397-408.
501 12. O'Shaughnessy J, Miles D, Vukelja S, Moiseyenko V, Ayoub JP, Cervantes G, et al. Superior survival
502 with capecitabine plus docetaxel combination therapy in anthracycline-pretreated patients with advanced
503 breast cancer: phase III trial results. J Clin Oncol. 2002;20(12):2812-23.
504 13. Pegram MD, Slamon DJ. Combination therapy with trastuzumab (Herceptin) and cisplatin for
505 chemoresistant metastatic breast cancer: evidence for receptor-enhanced chemosensitivity. Semin Oncol.
506 1999;26(4 Suppl 12):89-95.
507 14. Ravandi F, Cortes JE, Jones D, Faderl S, Garcia-Manero G, Konopleva MY, et al. Phase I/II study of
508 combination therapy with sorafenib, idarubicin, and cytarabine in younger patients with acute myeloid
509 leukemia. J Clin Oncol. 2010;28(11):1856-62.
510 15. Wu P, Nielsen TE, Clausen MH. Small-molecule kinase inhibitors: an analysis of FDA-approved
511 drugs. Drug Discov Today. 2016;21(1):5-10.
512 16. Linding R, Jensen LJ, Ostheimer GJ, van Vugt MA, Jorgensen C, Miron IM, et al. Systematic
513 discovery of in vivo phosphorylation networks. Cell. 2007;129(7):1415-26.
514 17. Bender C, Henjes F, Frohlich H, Wiemann S, Korf U, Beissbarth T. Dynamic deterministic effects
515 propagation networks: learning signalling pathways from longitudinal protein array data. Bioinformatics.
516 2010;26(18):i596-602.

517 18. Papin JA, Hunter T, Palsson BO, Subramaniam S. Reconstruction of cellular signalling networks and
518 analysis of their properties. Nature reviews. 2005;6(2):99-111.
519 19. Hashemikhabir S, Ayaz ES, Kavurucu Y, Can T, Kahveci T. Large-scale signaling network
520 reconstruction. IEEE/ACM Trans Comput Biol Bioinform. 2012;9(6):1696-708.
521 20. Basso K, Margolin AA, Stolovitzky G, Klein U, Dalla-Favera R, Califano A. Reverse engineering of
522 regulatory networks in human B cells. Nat Genet. 2005;37(4):382-90.
523 21. Alvarez MJ, Shen Y, Giorgi FM, Lachmann A, Ding BB, Ye BH, et al. Functional characterization of
524 somatic mutations in cancer using network-based inference of protein activity. Nat Genet.
525 2016;48(8):838-47.
526 22. MacKay DJC. Information theory, inference, and learning algorithms. Cambridge, UK ; New York:
527 Cambridge University Press; 2003. xii, 628 p. p.
528 23. Margolin AA, Nemenman I, Basso K, Wiggins C, Stolovitzky G, Dalla Favera R, et al. ARACNE: an
529 algorithm for the reconstruction of gene regulatory networks in a mammalian cellular context. BMC
530 bioinformatics. 2006;7 Suppl 1:S7.
531 24. Basso K, Saito M, Sumazin P, Margolin AA, Wang K, Lim WK, et al. Integrated biochemical and
532 computational approach identifies BCL6 direct target genes controlling multiple pathways in normal
533 germinal center B cells. Blood. 2010;115(5):975-84.
534 25. Della Gatta G, Palomero T, Perez-Garcia A, Ambesi-Impiombato A, Bansal M, Carpenter ZW, et al.
535 Reverse engineering of TLX oncogenic transcriptional networks identifies RUNX1 as tumor suppressor in
536 T-ALL. Nat Med. 2012;18(3):436-40.
537 26. Carro MS, Lim WK, Alvarez MJ, Bollo RJ, Zhao X, Snyder EY, et al. The transcriptional network for
538 mesenchymal transformation of brain tumours. Nature. 2010;463(7279):318-25.
539 27. Sonabend AM, Bansal M, Guarnieri P, Lei L, Amendolara B, Soderquist C, et al. The transcriptional
540 regulatory network of proneural glioma determines the genetic alterations selected during tumor
541 progression. Cancer Res. 2014;74(5):1440-51.
542 28. Aebersold R, Mann M. Mass-spectrometric exploration of proteome structure and function.
543 Nature. 2016;537(7620):347-55.
544 29. Gillet LC, Leitner A, Aebersold R. Mass Spectrometry Applied to Bottom-Up Proteomics: Entering
545 the High-Throughput Era for Hypothesis Testing. Annu Rev Anal Chem (Palo Alto Calif). 2016;9(1):449-72.
546 30. Huttlin EL, Ting L, Bruckner RJ, Gebreab F, Gygi MP, Szpyt J, et al. The BioPlex Network: A
547 Systematic Exploration of the Human Interactome. Cell. 2015;162(2):425-40.
548 31. Huttlin EL, Bruckner RJ, Paulo JA, Cannon JR, Ting L, Baltier K, et al. Architecture of the human
549 interactome defines protein communities and disease networks. Nature. 2017;545(7655):505-9.
550 32. Guo A, Villen J, Kornhauser J, Lee KA, Stokes MP, Rikova K, et al. Signaling networks assembled by
551 oncogenic EGFR and c-Met. Proc Natl Acad Sci U S A. 2008;105(2):692-7.
552 33. Giansanti P, Aye TT, van den Toorn H, Peng M, van Breukelen B, Heck AJ. An Augmented Multiple-
553 Protease-Based Human Phosphopeptide Atlas. Cell Rep. 2015;11(11):1834-43.
554 34. Lefebvre C, Rajbhandari P, Alvarez MJ, Bandaru P, Lim WK, Sato M, et al. A human B-cell
555 interactome identifies MYB and FOXM1 as master regulators of proliferation in germinal centers. Mol Syst
556 Biol. 2010;6:377.
557 35. Chudnovsky Y, Kim D, Zheng SY, Whyte WA, Bansal M, Bray MA, et al. ZFHX4 Interacts with the
558 NuRD Core Member CHD4 and Regulates the Glioblastoma Tumor-Initiating Cell State. Cell Rep.
559 2014;6(2):313-24.
560 36. Ying CY, Dominguez-Sola D, Fabi M, Lorenz IC, Hussein S, Bansal M, et al. MEF2B mutations lead
561 to deregulated expression of the oncogene BCL6 in diffuse large B cell lymphoma. Nat Immunol.
562 2013;14(10):1084-+.

563 37. Bisikirska B, Bansal M, Shen Y, Teruya-Feldstein J, Chaganti R, Califano A. Elucidation and
564 Pharmacological Targeting of Novel Molecular Drivers of Follicular Lymphoma Progression. Cancer Res.
565 2016;76(3):664-74.
566 38. Piovan E, Yu J, Tosello V, Herranz D, Ambesi-Impiombato A, Da Silva AC, et al. Direct reversal of
567 glucocorticoid resistance by AKT inhibition in acute lymphoblastic leukemia. Cancer Cell. 2013;24(6):766-
568 76.
569 39. Aytes A, Mitrofanova A, Lefebvre C, Alvarez MJ, Castillo-Martin M, Zheng T, et al. Cross-species
570 regulatory network analysis identifies a synergistic interaction between FOXM1 and CENPF that drives
571 prostate cancer malignancy. Cancer Cell. 2014;25(5):638-51.
572 40. Mitrofanova A, Aytes A, Shen C, Abate-Shen C, Califano A. A systems biology approach to predict
573 drug response for human prostate cancer based on in vivo preclinical analyses of mouse models. Cell
574 Reports. 2015;12:1–12.
575 41. Talos F, Mitrofanova A, Bergren SK, Califano A, Shen MM. A computational systems approach
576 identifies synergistic specification genes that facilitate lineage conversion to prostate tissue. Nature
577 communications. 2017;8:14662.
578 42. Walsh LA, Alvarez MJ, Sabio EY, Reyngold M, Makarov V, Mukherjee S, et al. An Integrated Systems
579 Biology Approach Identifies TRIM25 as a Key Determinant of Breast Cancer Metastasis. Cell Rep.
580 2017;20(7):1623-40.
581 43. Rodriguez-Barrueco R, Yu J, Saucedo-Cuevas LP, Olivan M, Llobet-Navas D, Putcha P, et al.
582 Inhibition of the autocrine IL-6-JAK2-STAT3-calprotectin axis as targeted therapy for HR-/HER2+ breast
583 cancers. Genes Dev. 2015;29(15):1631-48.
584 44. Putcha P, Yu J, Rodriguez-Barrueco R, Saucedo-Cuevas L, Villagrasa P, Murga-Penas E, et al. HDAC6
585 activity is a non-oncogene addiction hub for inflammatory breast cancers. Breast Cancer Res.
586 2015;17(1):149.
587 45. Davoli A, Hocevar BA, Brown TL. Progression and treatment of HER2-positive breast cancer.
588 Cancer Chemother Pharmacol.65(4):611-23.
589 46. Guo L, Kozlosky CJ, Ericsson LH, Daniel TO, Cerretti DP, Johnson RS. Studies of ligand-induced site-
590 specific phosphorylation of epidermal growth factor receptor. Journal of the American Society for Mass
591 Spectrometry. 2003;14(9):1022-31.
592 47. Okamoto I. Epidermal growth factor receptor in relation to tumor development: EGFR-targeted
593 anticancer therapy. FEBS J.277(2):309-15.
594 48. Wang S, Placzek WJ, Stebbins JL, Mitra S, Noberini R, Koolpe M, et al. Novel targeted system to
595 deliver chemotherapeutic drugs to EphA2-expressing cancer cells. J Med Chem. 2012;55(5):2427-36.
596 49. Birtwistle MR, Hatakeyama M, Yumoto N, Ogunnaike BA, Hoek JB, Kholodenko BN. Ligand-
597 dependent responses of the ErbB signaling network: experimental and modeling analyses. Mol Syst Biol.
598 2007;3:144.
599 50. Rikova K, Guo A, Zeng Q, Possemato A, Yu J, Haack H, et al. Global survey of phosphotyrosine
600 signaling identifies oncogenic kinases in lung cancer. Cell. 2007;131(6):1190-203.
601 51. Soda M, Choi YL, Enomoto M, Takada S, Yamashita Y, Ishikawa S, et al. Identification of the
602 transforming EML4-ALK fusion gene in non-small-cell lung cancer. Nature. 2007;448(7153):561-6.
603 52. Laurent C, Do C, Gascoyne RD, Lamant L, Ysebaert L, Laurent G, et al. Anaplastic lymphoma kinase-
604 positive diffuse large B-cell lymphoma: a rare clinicopathologic entity with poor prognosis. J Clin Oncol.
605 2009;27(25):4211-6.
606 53. Janoueix-Lerosey I, Lequin D, Brugieres L, Ribeiro A, de Pontual L, Combaret V, et al. Somatic and
607 germline activating mutations of the ALK kinase receptor in neuroblastoma. Nature. 2008;455(7215):967-
608 70.
609 54. Sokai A, Enaka M, Sokai R, Mori S, Mori S, Gunji M, et al. Pulmonary Inflammatory Myofibroblastic
610 Tumor Harboring EML4-ALK Fusion Gene. Jpn J Clin Oncol. 2014;44(1):93-6.

611 55. Bender C, Henjes F, Frohlich H, Wiemann S, Korf U, Beissbarth T. Dynamic deterministic effects
612 propagation networks: learning signalling pathways from longitudinal protein array data. Bioinformatics.
613 2010;26(18):i596-i602.
614 56. Koivunen JP, Mermel C, Zejnullahu K, Murphy C, Lifshits E, Holmes AJ, et al. EML4-ALK fusion gene
615 and efficacy of an ALK kinase inhibitor in lung cancer. Clin Cancer Res. 2008;14(13):4275-83.
616 57. TCGA-Consortium. Comprehensive genomic characterization defines human glioblastoma genes
617 and core pathways. Nature. 2008;455(7216):1061-8.
618 58. Crystal AS, Shaw AT. Variants on a theme: a biomarker of crizotinib response in ALK-positive non-
619 small cell lung cancer? Clin Cancer Res. 2012;18(17):4479-81.
620 59. Shaw AT, Solomon B. Targeting anaplastic lymphoma kinase in lung cancer. Clin Cancer Res.
621 2011;17(8):2081-6.
622 60. . !!! INVALID CITATION !!! [24].
623 61. Voena C, Di Giacomo F, Panizza E, D'Amico L, Boccalatte FE, Pellegrino E, et al. The EGFR family
624 members sustain the neoplastic phenotype of ALK+ lung adenocarcinoma via EGR1. Oncogenesis.
625 2013;2:e43.
626 62. Chan BA, Hughes BG. Targeted therapy for non-small cell lung cancer: current standards and the
627 promise of the future. Transl Lung Cancer Res. 2015;4(1):36-54.
628 63. Landi L, Minuti G, D'Incecco A, Cappuzzo F. Targeting c-MET in the battle against advanced
629 nonsmall-cell lung cancer. Curr Opin Oncol. 2013;25(2):130-6.
630 64. Borisy AA, Elliott PJ, Hurst NW, Lee MS, Lehar J, Price ER, et al. Systematic discovery of
631 multicomponent therapeutics. Proc Natl Acad Sci U S A. 2003;100(13):7977-82.
632 65. Chou TC. Drug Combination Studies and Their Synergy Quantification Using the Chou-Talalay
633 Method. Cancer research. 2010;70(2):440-6.
634 66. Zhang G, Fang B, Liu RZ, Lin H, Kinose F, Bai Y, et al. Mass spectrometry mapping of epidermal
635 growth factor receptor phosphorylation related to oncogenic mutations and tyrosine kinase inhibitor
636 sensitivity. J Proteome Res. 2011;10(1):305-19.
637 67. Valencia K, Ormazabal C, Zandueta C, Luis-Ravelo D, Anton I, Pajares MJ, et al. Inhibition of
638 collagen receptor discoidin domain receptor-1 (DDR1) reduces cell survival, homing, and colonization in
639 lung cancer bone metastasis. Clin Cancer Res. 2012;18(4):969-80.
640 68. Scott J, Ideker T, Karp RM, Sharan R. Efficient algorithms for detecting signaling pathways in
641 protein interaction networks. Journal of computational biology : a journal of computational molecular cell
642 biology. 2006;13(2):133-44.
643 69. Steffen M, Petti A, Aach J, D'Haeseleer P, Church G. Automated modelling of signal transduction
644 networks. BMC bioinformatics. 2002;3:34.
645 70. Kelley BP, Sharan R, Karp RM, Sittler T, Root DE, Stockwell BR, et al. Conserved pathways within
646 bacteria and yeast as revealed by global protein network alignment. Proceedings of the National Academy
647 of Sciences of the United States of America. 2003;100(20):11394-9.
648 71. Shimoni Y, Fink MY, Choi SG, Sealfon SC. Plato's cave algorithm: inferring functional signaling
649 networks from early gene expression shadows. PLoS Comput Biol. 2010;6(6):e1000828.
650 72. Budak G, Eren Ozsoy O, Aydin Son Y, Can T, Tuncbag N. Reconstruction of the temporal signaling
651 network in Salmonella-infected human cells. Front Microbiol. 2015;6:730.
652 73. Zhang QC, Petrey D, Deng L, Qiang L, Shi Y, Thu CA, et al. Structure-based prediction of protein-
653 protein interactions on a genome-wide scale. Nature. 2012;490(7421):556-60.
654 74. Lamb J, Crawford ED, Peck D, Modell JW, Blat IC, Wrobel MJ, et al. The Connectivity Map: using
655 gene-expression signatures to connect small molecules, genes, and disease. Science.
656 2006;313(5795):1929-35.
657 75. Mok TS, Wu YL, Thongprasert S, Yang CH, Chu DT, Saijo N, et al. Gefitinib or carboplatin-paclitaxel
658 in pulmonary adenocarcinoma. The New England journal of medicine. 2009;361(10):947-57.

659 76. Steuer R, Kurths J, Daub CO, Weise J, Selbig J. The mutual information: detecting and evaluating
660 dependencies between variables. Bioinformatics. 2002;18 Suppl 2:S231-40.
661 77. Gandhi J, Zhang JL, Xie Y, Soh J, Shigematsu H, Zhang W, et al. Alterations in Genes of the EGFR
662 Signaling Pathway and Their Relationship to EGFR Tyrosine Kinase Inhibitor Sensitivity in Lung Cancer Cell
663 Lines. PloS one. 2009;4(2).

664

Figure Legends

Figure 1. Framework for the reverse engineering of TK signaling networks from phosphoproteomic profiles.

(A) Schematic diagram of a **TK→S** interaction. The non-phosphorylated kinase is inactive in terms of phosphorylating a substrate, while the active isoform successfully phosphorylates the substrate. **(B)** Schematic diagram showing the correlation between TK phosphorylation and that of its potential substrates. The first two rows in the heatmap show proteins representing candidate TK substrates **(C)** Illustration of the pARACNe framework including 6 steps. Step-1 depicts peptides collection from primary lung cancer tissue and cell lines for whole phosphrtyrosine proteomics quantification. Step-2 depicts inferences of TK→S interactions using Mutual Information by Step-3 Naïve-Bayes estimator and Step-4 of the iterative quantile discretization methods. Step-5 and 6 depict network pruning and bootstrapping to construct final network. **(C)**. Workflow of pARACNe from LC-MS/MS data normalization, IQD process, MI calculation, DPI process, bootstrapping to network consolidation.

Figure 2. Predicted TK-TK network and validation of EGFR and c-MET prediction

(A) pARACNe-inferred densely inter-connected TK-TK network, with red nodes representing candidate TKs involved in auto-phosphorylation, where the phospho-state of a tyrosine is correlated with the phospho-state of a different tyrosine on the same TK protein. **(B)** pARACNe-inferred EGFR and **(C)** c-MET substrate overlap with SILAC-based and Database reported substrates, respectively.

Figure 3. Inference of Master Regulator and combination

(A). Schema of Master Regulator analysis in lung cancer using pVIPER. Prioritized Master Regulators **(B)** and Prioritized Master Regulator Pairs **(C)** as significantly activated (red circle) or

689 de-activated (blue) in different lung cancer cell lines (column). Red color represents an enrichment
690 of substrates hyper-phosphorylation by a Master Regulator or Master Regulator Pairs. Blue color
691 represents that of hypo-phosphorylation.

692 **Figure 4. Experimental validation of EGFR and c-MET combination by colony**
693 **formation assay**

694 **(A)** Colony formation assay schema. **(B)** shows the image of long-term EGFR and c-MET double
695 inhibition effects in HCC78 cell line with different treatments. **(C)** shows long-term clony formation
696 data for 14 cell lines with different EGFR, BRAF and KRAS genomic mutation status.

697 **Figure 5. MTT Assay validation of EGFR and c-MET combination**

698 **(A)**. MTT assay experimental schema. **(B)** MTT assay of HCC78 cell line shows synergistic effects
699 of Crizotinib and Erlotinib treatment. **(C)** shows short-term effects of EGFR and c-MET inhibitors'
700 combination index in 11 cell lines include 2 control cell lines (red).

701 **Figure 6. Master Regulating peptides in primary lung cancer samples**

702 EGFR and c-MET co-regulate in three scenarios **(A)** when their common substrates are
703 hyperphosphrylated, the patient responds to combination treatment well; **(B)** when most EGFR
704 substrates are hyper-phosphorylated, the patient responds to EGFR inhibitor; **(C)** when
705 substrates of both EGFR and c-MET are mostly hypophosphorylated, the patient does not
706 respond. **(D)** show the Master Regulator and Master Regulator Pairs regulating hyper/hypo-
707 phosphorylation of their network substrates in each primary samples.

708

709 # Methods and Data

710 ***Phosphoproteomic Data***

711 The previously published phosphoproteomic data used to reconstruct signaling network was
712 download from (50). This dataset, representing the abundance of phospho-tyrosine containing
713 peptides, was obtained by tandem mass spectrometry analysis of 46 non-small cell lung cancer
714 (NSCLC) cell lines, 151 NSCLC tumors, and 48 normal lung tissue samples.
715 Immunohistochemistry and a phospho-tyrosine specific antibody were used to screen 96 paraffin-
716 embedded, formalin fixed tissue samples from NSCLC patients as described by Rikova et al.(50).
717 About 30% of tumors showed high-levels of phospho-tyrosine expression. Immunoblotting of 46
718 NSCLC cell lines with a phospho-tyrosine specific antibody also showed heterogeneous reactivity
719 especially in the molecular weight range characteristic of receptor tyrosine kinases.

720 Since phospho-tyrosine represents less than 1% of the cellular phosphoproteome, as determined
721 by tandem mass spectrometry (MS/MS), and is difficult to analyze by conventional methods,
722 immuno-affinity purification was performed with a phospho-tyrosine antibody to enrich for
723 phospho-tyrosine containing peptides prior to tandem mass spectrometry. All tumors were
724 identified as NSCLC based on standard pathology. Only those tumors with greater than 50% of
725 cancer cells were considered for further analysis. NSCLC cell lines were grown overnight in low
726 serum to reduce background phosphorylation from culture conditions.

727 Tandem MS profiling identified 3920 tyrosine phosphorylation sites on approximately 2600
728 different proteins. 85% of these sites appeared to be novel when compared against PhosphoSite
729 (http://www.phosphosite.org), a comprehensive resource of known phosphorylation sites.

730 ***pARACNe Algorithm***

731 ARACNe is originally designed for gene expression data, where expression of genes is usually
732 continuous and non-sparse. Quantitative data obtained from label-free LC-MS/MS by data-
733 dependent acquisition via spectral counting is discrete and very sparse, with many
734 phosphopeptides counts not observed for multiple peptides in each sample causing the current
735 version of ARACNe to be not suitable for this data, which thus required major modifications to
736 handle discrete data. To handle discrete abundances, we modified the mutual information
737 computation approach from a kernel density estimation based method to a Naïve based
738 estimation of mutual information, which is a histogram based technique(76). Briefly, consider a
739 collection of *N* simultaneous measurements of two genes X and Y. Data is partitioned into M
740 discrete bins a_i, and k_i denotes the number of measurements that lie within the bin a_i. The
741 probabilities $p(a_i)$ are then approximated by the corresponding relative frequencies of
742 occurrence $p(a_i) \rightarrow \frac{k_i}{N}$ and the mutual information $I(X,Y)$ between datasets X and Y is
743 expressed as

744 $$I(X,Y) = \log N + \frac{1}{N}\sum_{ij} k_{ij} \log \frac{k_{ij}}{k_i k_j}$$

745 Here k_{ij} denotes the number of measurements where X lies in a_i and Y in a_j and *N* total number
746 of samples.

747 Accuracy of mutual information is dependent on correct numbers of bins, M. To find the optimal
748 number of bins we applied ARACNe on the whole dataset by varying M from 1 to 20 and testing
749 the connections in predicted sub-network against the set of known connections (gold standard)
750 from databases (phosphoDB) (33).

751 In case of continuous data, partitioning can be achieved by dividing the range of data into M
752 equally spaced distance bins. Our data being discrete, equally spaced partitioning was not
753 possible. So, to overcome this problem, we used an iterative approach of partitioning **(Fig. 1C,**
754 **Fig. S1A)**. The basic idea is to divide the number of N data points into M with each bin containing
755 equal number of data point. If the data point(s) with the same value falls into consecutive bin(s),
756 we put those data point(s) into current bin and repartition the remaining points into remaining
757 number of bins. We keep iterating this till we finish either the bins or there are no more data points
758 to bin. For example, in **Fig. S1A**, we initially partition N points into 4 bins. The data points with 0
759 value does not fit into first bin and falls into subsequent bins, so we assign all data points with 0
760 value into first bin and repartition the remaining points into 3 bins. We keep on doing this process
761 till we achieve 4 bins.

762 To evaluate initial performance and decide number of bins, we computed the network among all
763 tyrosine kinases and substrates, parsed the sub-network between 49 tyrosine kinases and 114
764 substrates which were present in PhosphoSite database and compared the results with the
765 connections present in database. From our analysis, we found that M=10 to be an optimal number
766 **(Fig. S1B)** which gave us precision of 14% and sensitivity of 24%. This precision is an
767 underestimate of real precision as in the gold standard many interactions are not present.

768 ***Master Regulator Analysis***

769 To discover the master regulator in various cell lines, we interrogated the network obtained from
770 pARACNe using a novel algorithm, VIPER (Virtual Proteomics by Enriched Regulon analysis)
771 (21), designed to infer kinases that are key players in a particular cell line. Protein activity is a
772 good indicator of key kinases in a particular phenotype but often phosphorylated state of a protein
773 is not sufficient to determine its activity both due to measurement noise in phosphorylated state
774 as well as LC-MS/MS technique noise. To overcome this problem, VIPER infers kinase activity

775 from the global kinase substrate relationship and its biological relevance by overlapping this
776 information in a particular phenotype-specific program.

777 VIPER requires a network model and signature of the phenotype transition (i.e., all genes ranked
778 by their differential phosphorylation in two phenotypes). Here, the signature, S_{kin}, was obtained
779 by t-test analysis by comparing each cell line against all normal samples. First, we associate each
780 kinase with positive and negative activity targets, by computing the correlation between each
781 kinase and its predicted substrates and selecting only those substrates which had a significant
782 correlation (p-value ≤ 0.05, Bonferroni corrected). Second, for each kinase we computed an
783 *activity* by measuring the enrichment of the S_{kin} signature in predicted substrates list, separately
784 for both positive and negative correlated, (S_{kin}-*enrichment*). Enrichment was computed by Gene
785 Set Enrichment Analysis (GSEA). Since very small percentage of kinases are found to have
786 negative correlation, we did not use those interactions to evaluate enrichment.

787 ***Cell Culture***

788 All cell lines were grown in RPMI-1640 with 5% fetal bovine serum and incubated at 37ºC in a
789 humidified atmosphere containing 5% CO_2. Cell lines were fingerprinted using the Perplex 1.2
790 system (Promega, Madison, WI). Fingerprints were compared to those generated at ATCC and/or
791 our internal database.

792 ***MTS Assays***

793 Short term MTS assays (CellTiter 96® AQ_{ueous} One Solution Cell Proliferation Assay, Promega,
794 Madison WI) were performed as previously described in (77). Specifically, each drug
795 concentration is octuplicated and the mean with standard deviation of all replicates were used to
796 generate a curve to allow calculation of the drug IC50 (Inhibitory Concentration of 50%) value.
797 The assays were repeated at least 3 times and the IC50s are the average of all replicates.

798

799 ***Colony-formation Assays***

800 Long term colony formation assays were performed in triplicate in 6-well plates. Cells were added
801 to media containing drug and incubated for 1-2 weeks such that control wells (no drug) contained
802 colonies of 50-70 cells each. At such time media was removed and all wells stained with a solution
803 containing 0.5% crystal violet and 6% glutaraldehyde for 1 hour. The plates were then rinsed,
804 dried, and colonies were manually counted.

805 ***SILAC Experiments***

806 EGFR SILAC experiment was performed in H3255 cell line by treating samples with Gefitinib. c-
807 MET SILAC experiment was performed in c-MET-driven gastric cancer cell line, MKN45, by using
808 c-MET inhibitor Su11274. For both genes, cells were treated with inhibitors for 3 and 24hr. For
809 control, cells were grown in same conditions but were not treated with the drug. For our
810 comparison we combined the peptides, which were differentially obtained between treated and
811 untreated samples, for 3 and 24 hr. More details about the experiment can be obtained from Guo
812 et al (32).

813 **Gold standard**: In PhosphoSite database, there were 282 connections between 49 tyrosine
814 kinases and 114 substrates.

815

816 ## Supplemental Information

817 ***Fig. S1. Performance of the pARACNe Algorithm.***

818 **(A).** To select optimal bin number in pARACNe algorithm, precision and recall curves for various
819 number of bins were computed. Black curve is when no binning of data is done. When using 10
820 bins, the algorithm achieved the best performance.

821 ***Table S1. pARACNe-inferred TK-peptides/substrate-peptides Interaction Network.***

822 ***Table S2. pARACNe-inferred TK-Protein/Substrate Interaction Network.***

823 ***Table S3. Colony Formation Assay and MTS Assay Results.***

824

Figure 1

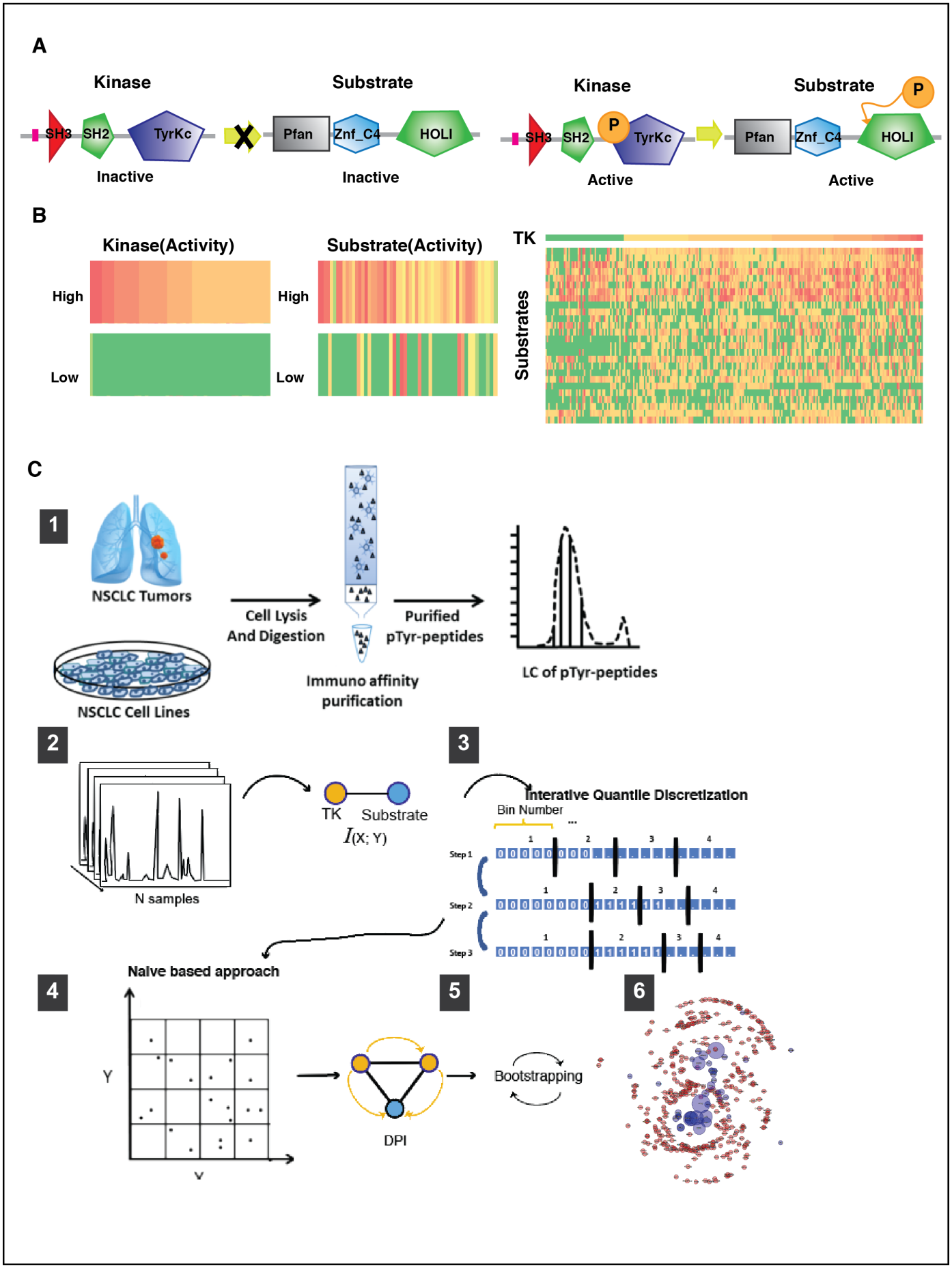
A
Kinase
Substrate
SH3
SH2
TyrKc
Pfan
Znf_C4
HOLI
Inactive
Inactive
Kinase
Substrate
P
Active
Active
B
Kinase(Activity)
Substrate(Activity)
High
Low
High
Low
TK
Substrates
C
1
NSCLC Tumors
NSCLC Cell Lines
Cell Lysis
And Digestion
Immuno affinity
purification
Purified
pTyr-peptides
LC of pTyr-peptides
2
N samples
TK
Substrate
I(X; Y)
3
Interative Quantile Discretization
Bin Number
Step 1
Step 2
Step 3
4
Naive based approach
Y
X
DPI
5
Bootstrapping
6

Figure 2

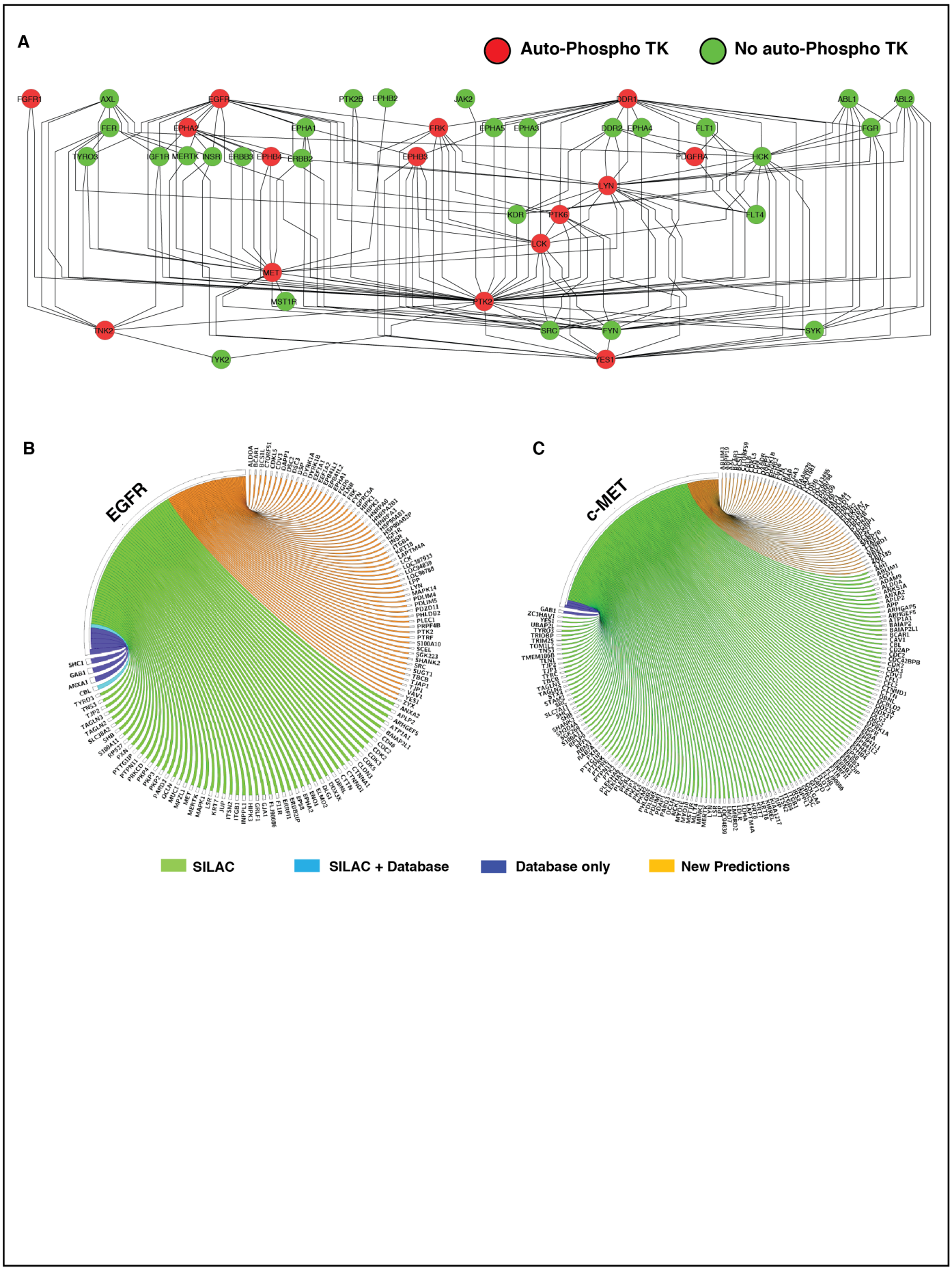
A
Auto-Phospho TK
No auto-Phospho TK
FGFR1
AXL
EGFR
PTK2B
EPHB2
JAK2
DDR1
ABL1
ABL2
FER
EPHA2
EPHA1
FRK
EPHA5
EPHA3
DDR2
EPHA4
FLT1
FGR
TYRO3
IGF1R
MERTK
INSR
ERBB3
EPHB4
ERBB2
EPHB3
PDGFRA
HCK
LYN
KDR
PTK6
FLT4
LCK
MET
MST1R
PTK2
TNK2
SRC
FYN
SYK
TYK2
YES1
B
EGFR
C
c-MET
SILAC
SILAC + Database
Database only
New Predictions

Figure 3

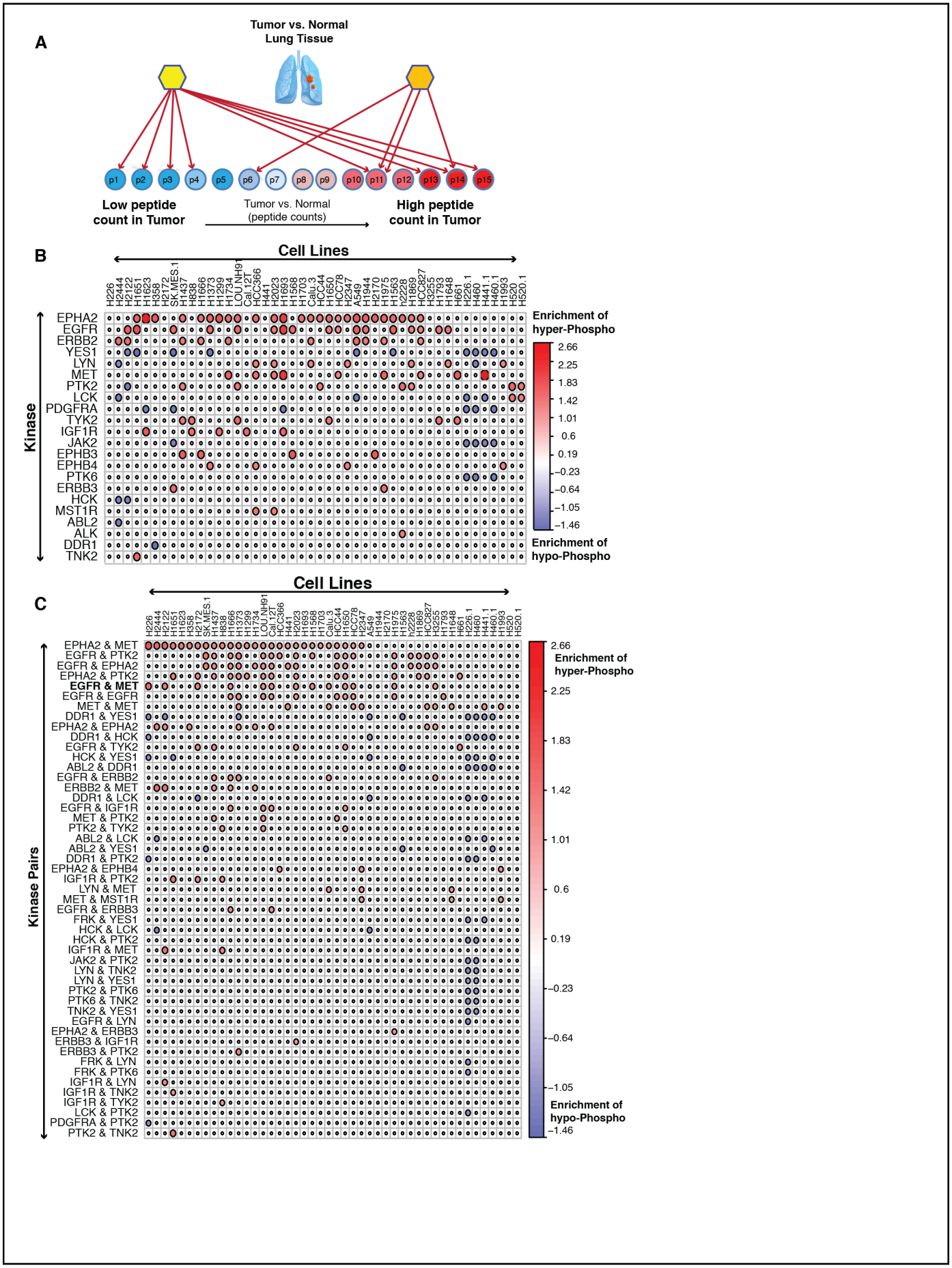
A
Tumor vs. Normal
Lung Tissue
p1 p2 p3 p4 p5 p6 p7 p8 p9 p10 p11 p12 p13 p14 p15
Low peptide count in Tumor
Tumor vs. Normal (peptide counts)
High peptide count in Tumor
B
Cell Lines
Kinase
EPHA2
EGFR
ERBB2
YES1
LYN
MET
PTK2
LCK
PDGFRA
TYK2
IGF1R
JAK2
EPHB3
EPHB4
PTK6
ERBB3
HCK
MST1R
ABL2
ALK
DDR1
TNK2
Enrichment of hyper-Phospho
2.66
2.25
1.83
1.42
1.01
0.6
0.19
−0.23
−0.64
−1.05
−1.46
Enrichment of hypo-Phospho
C
Cell Lines
Kinase Pairs
EPHA2 & MET
EGFR & PTK2
EGFR & EPHA2
EPHA2 & PTK2
EGFR & MET
EGFR & EGFR
MET & MET
DDR1 & YES1
EPHA2 & EPHA2
DDR1 & HCK
EGFR & TYK2
HCK & YES1
ABL2 & DDR1
EGFR & ERBB2
ERBB2 & MET
DDR1 & LCK
EGFR & IGF1R
MET & PTK2
PTK2 & TYK2
ABL2 & LCK
ABL2 & YES1
DDR1 & PTK2
EPHA2 & EPHB4
IGF1R & PTK2
LYN & MET
MET & MST1R
EGFR & ERBB3
FRK & YES1
HCK & LCK
HCK & PTK2
IGF1R & MET
JAK2 & PTK2
LYN & TNK2
LYN & YES1
PTK2 & PTK6
PTK6 & TNK2
TNK2 & YES1
EGFR & LYN
EPHA2 & ERBB3
ERBB3 & IGF1R
ERBB3 & PTK2
FRK & LYN
FRK & PTK6
IGF1R & LYN
IGF1R & TNK2
IGF1R & TYK2
LCK & PTK2
PDGFRA & PTK2
PTK2 & TNK2
Enrichment of hyper-Phospho
2.66
2.25
1.83
1.42
1.01
0.6
0.19
−0.23
−0.64
−1.05
−1.46
Enrichment of hypo-Phospho

Figure 4

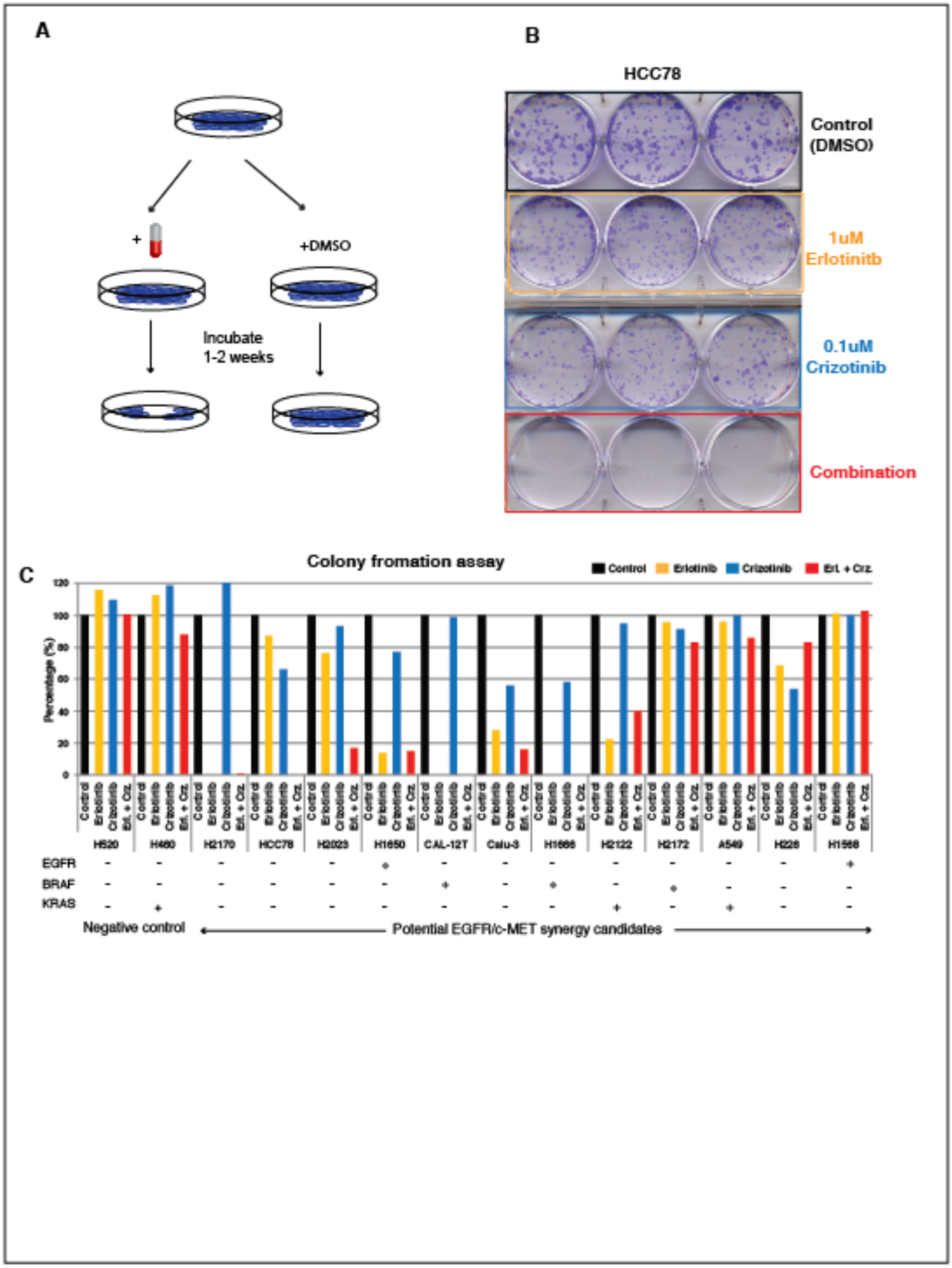
A
+
+DMSO
Incubate
1-2 weeks
B
HCC78
Control
(DMSO)
1uM
Erlotinitb
0.1uM
Crizotinib
Combination
C
Colony fromation assay
Control
Erlotinib
Crizotinib
Erl. + Crz.
Percentage (%)
120
100
80
60
40
20
0
H520
H460
H2170
HCC78
H2023
H1650
CAL-12T
Calu-3
H1666
H2122
H2172
A549
H226
H1568
EGFR
BRAF
KRAS
Negative control
Potential EGFR/c-MET synergy candidates

Figure 5

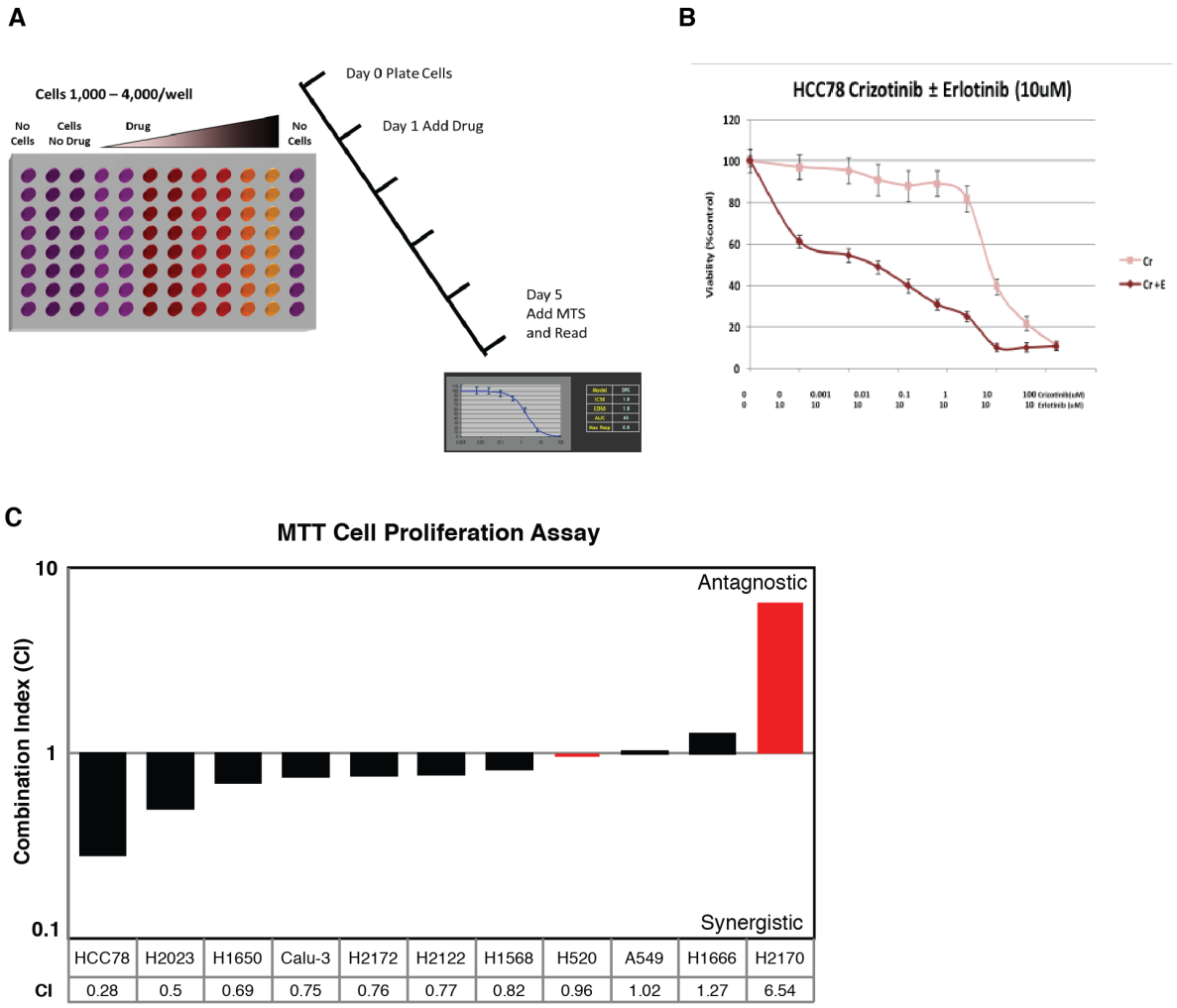
A
Cells 1,000 – 4,000/well
No Cells
Cells No Drug
Drug
No Cells
Day 0 Plate Cells
Day 1 Add Drug
Day 5 Add MTS and Read
B
HCC78 Crizotinib ± Erlotinib (10uM)
Viability (%control)
120
100
80
60
40
20
0
Cr
Cr+E
C
MTT Cell Proliferation Assay
Combination Index (CI)
10
1
0.1
Antagnostic
Synergistic
HCC78 H2023 H1650 Calu-3 H2172 H2122 H1568 H520 A549 H1666 H2170
CI 0.28 0.5 0.69 0.75 0.76 0.77 0.82 0.96 1.02 1.27 6.54

Figure 6

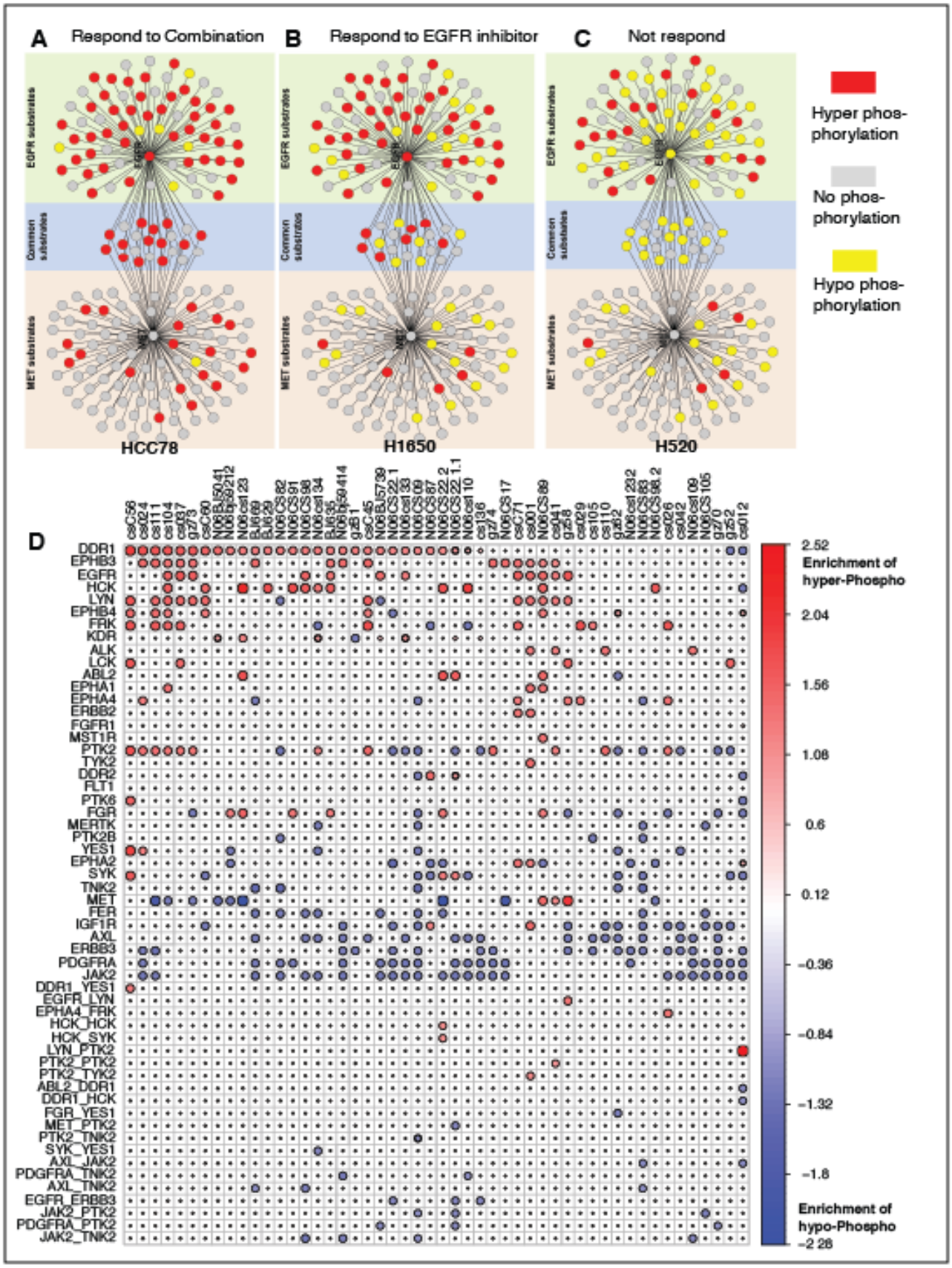
A
Respond to Combination
B
Respond to EGFR inhibitor
C
Not respond
EGFR substrates
Common substrates
MET substrates
HCC78
H1650
H520
Hyper phos-phorylation
No phos-phorylation
Hypo phos-phorylation
D
DDR1
EPHB3
EGFR
HCK
LYN
EPHB4
FRK
KDR
ALK
LCK
ABL2
EPHA1
EPHA4
ERBB2
FGFR1
MST1R
PTK2
TYK2
DDR2
FLT1
PTK6
FGR
MERTK
PTK2B
YES1
EPHA2
SYK
TNK2
MET
FER
IGF1R
AXL
ERBB3
PDGFRA
JAK2
DDR1_YES1
EGFR_LYN
EPHA4_FRK
HCK_HCK
HCK_SYK
LYN_PTK2
PTK2_PTK2
PTK2_TYK2
ABL2_DDR1
DDR1_HCK
FGR_YES1
MET_PTK2
PTK2_TNK2
SYK_YES1
AXL_JAK2
PDGFRA_TNK2
AXL_TNK2
EGFR_ERBB3
JAK2_PTK2
PDGFRA_PTK2
JAK2_TNK2
2.52
Enrichment of hyper-Phospho
2.04
1.56
1.08
0.6
0.12
−0.36
−0.84
−1.32
−1.8
Enrichment of hypo-Phospho
−2.28